

Effect of Liner Cooling Flow on Combustor Emissions for Commercial Supersonics Technology

Kumud Ajmani^{1,}
Jeffrey P. Moder²*

¹*Engine Combustion Branch, HX5 LLC, Cleveland OH, USA*

²*Chief, Engine Combustion Branch, NASA Glenn Research Center, Cleveland OH, USA*

**Corresponding Author Email: kumud.ajmani-1@nasa.gov*

Abstract: An overview is provided of a parametric study conducted to study the effect of liner cooling airflow rates on NO_x emissions of a seven-element lean-direct injection (LDI) module with radial airflow main swirlers. The goal of the CFD study was to determine the increase in cooling flow rate at which the NO_x emissions would exceed 20% of the predicted emissions with zero liner cooling flow. The Open version of the National Combustion Code (OpenNCC) was used to perform two-phase reacting flow computations with a new LDI injection module design with radial airflow swirlers instead of axial airflow swirlers. CFD analysis with OpenNCC predicted a 20% increase in EINO_x emissions was reached when the liner cooling airflow rate was increased to 15% of the baseline combustor airflow rate. The liner cooling flow rate was predicted to have a non-linear effect on increase in overall EINO_x of the seven element LDI injection module.

Keywords: *Gas Turbine Combustion, Fuels, Computational Fluid Dynamics, Supersonics, Lean Direct Injection*

1.0 Introduction

Commercial Supersonic Technology (CST) aircraft are projected to spend most of their cruising flight envelope at relatively higher altitudes and higher combustor operating temperatures as compared to current subsonic aircraft. The combination of higher cruise operating temperatures at higher altitudes, combined with the goal of ultra-low NO_x emissions, creates unique design challenges for CST combustors [1]. In addition to reducing NO_x and CO emissions in high-altitude flight, reducing carbon emissions by using SAFs is also a significant research area under NASA's CST project. NASA Glenn's Open National Combustion Code (OpenNCC) has been used for multiple CFD studies of Lean Direct Injection (LDI) redesigns [2] and impacts of SAF fuel blends on emissions [3,4] to support the CST project.

This paper describes an ongoing CFD effort focused on redesigning the injector modules of an existing Lean Direct Injection (LDI) combustor, with the goal of attaining an EINO_x of 10 or below at supersonic cruise conditions. Three previous CFD studies have described injector redesign and impacts of fuels on emissions and flame-structure to support commercial supersonics flight emissions goals: (a) evaluate impacts of three different, unblended fuels: 'average' Jet-A (A2), RP-2 and SASOL iso-paraffin kerosene (IPK) [6], (b) evaluate impacts of arbitrary fuel blending ratios of 'average' Jet-A (A2) and GEVO Alcohol-to-Jet (ATJ or C1) fuel [7], and (c) redesign of a seven-element LDI module by replacing axial inflow main swirlers with radial airflow swirlers [8]. The configuration used for the current parametric study was the radial inflow variant of a third generation LDI combustor designed and tested for subsonic flight under NASA's N+3 project by Woodward FST Inc [5]. While the N+3 combustor was not optimized for a supersonic aircraft cycle, it provided a realistic starting point to attempt a low-NO_x combustor redesign to meet supersonic cruise emissions goals of NASA's Commercial Supersonics Technology (CST) project.

2.0 LDI Combustor Flametube Redesign using OpenNCC

Figure 1 shows a representation of the dome-layout of the three cups of a nineteen-injector element arranged in a 7-5-7 element pattern, as tested at NASA GRC. The flametube was designed by Woodward FST Inc, to meet performance and emissions requirements for subsonic aviation under NASA’s N+3 Advanced Air Transport Technology (AATT) program. A limited set of emissions data was also obtained for certain operating points corresponding to a NASA Supersonic Cycle designed for Commercial Supersonics Technology (CST) applications [5]. The nominal supersonics cruise conditions for this NASA engine cycle were $P_3=15.9\text{bar}$ (234psi), $T_3=884\text{K}$ (1132F), equivalence ratio (ϕ)=0.43 (Fuel-Air Ratio, FAR=0.0295) and combustor pressure-drop, $\Delta p=3.5\%$ [4]. Design details of one of the seven-element cups with axially-bladed airflow swirlers used in the six outer (main) elements, and a corresponding mesh for CFD analysis, are also shown in figure 1.

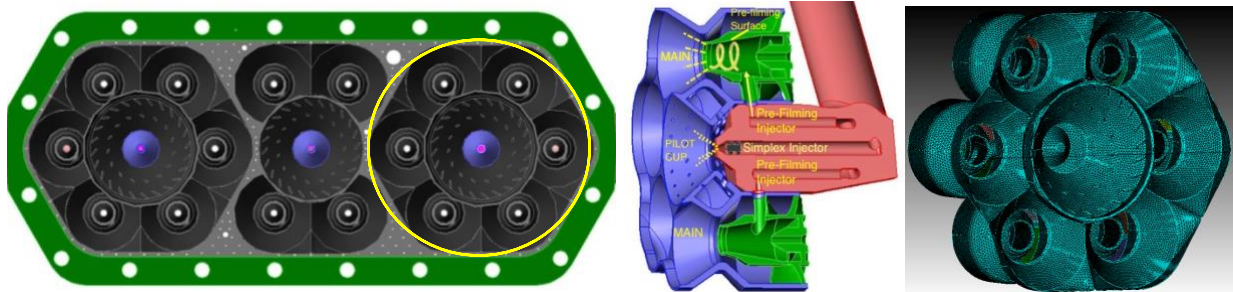


Figure 1. ‘Baseline’ LDI-3 Design: Dome-layout with alternating seven- and five-element cups for an LDI-3 injector array (left), with seven-element cup; details of the ‘axial-bladed’ seven-element cup with six outer mains and center pilot (center); OpenNCC CFD surface mesh for seven-element configuration (right)

In recent work, results were reported on a CFD analysis of the effects on flame structure and emissions of replacing the axial-bladed six main swirlers of the ‘baseline’ N+3 subsonics design, with radial-inflow injection elements for potential NO_x reduction in supersonics applications (Figure 2). Two different variations of the radial-airflow swirlers, labeled ‘co-rotating’ and ‘counter-rotating’ configurations, depending on the relative swirl direction of the ‘inner’ and ‘outer’ swirler passages of the six main elements (see table 1) were studied with NASA Glenn’s OpenNCC code [6]. The co-rotating swirler design was predicted to have 20% lower EINO_x at supersonics cruise conditions and was thus selected for the liner-cooling flow parametric study in this paper.

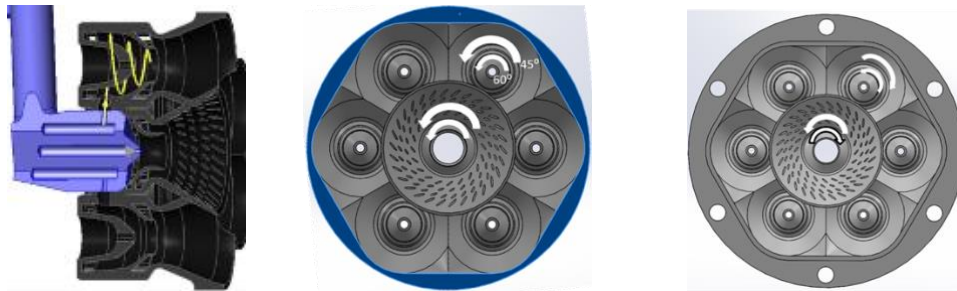


Figure 2. New LDI-4 Design: Dome-layout of ‘radial airflow’ seven-element cup (left); co-rotating radial-airflow configuration (center) and counter-rotating radial-airflow configuration (right)

Radial Airflow (LDI-4)	Mains Outer 45° / Inner 60°	Pilot Outer / Inner Row	Pilot Cooling Rows
Co-Rotating Design	CCW / CCW	CCW / CCW	CW
Counter-Rotating Design	CW / CCW	CCW / CW	CCW

Table 1. Orientation of radial airflow passages for six main elements, pilot element, and pilot cooling flow holes. CCW, CW: Counter-clockwise, Clockwise swirl (aft looking upstream)

3.0 CFD Assessment of Liner Cooling Flow Rate on NOx Emissions

A newly radial-swirler airflow injector design formulated by Woodward FST, Inc was evaluated with the OpenNCC code to study the effects of liner-cooling air-flow rates on flame-structure and EINOx emissions for a commercial supersonics cruise condition. The CFD parametric study used lagrangian-spray modeling (for the liquid phase droplets) [7] and a HyChem skeletal-kinetics mechanism [8] for ‘average’ Jet-A fuel. A Flamelet-Progress Variable (FPV) combustion model [9] was used to compute the two-phase flow combustion flow. The FPV model has recently been extended to a Multi-Time Scale Flamelet Progress Variable (MTS-FPV) approach [10] in order to reduce the computation time needed to obtain convergence of the NOx species in typical gas-turbine combustors.

With the MTS-FPV approach, the primary flame and the NOx production are decoupled due to the disparate time scales associated with each process. A multiphase flamelet progress variable approach is employed for the primary flame and the NOx species are transported independently as separate scalars. Detailed NOx chemistry is employed through the use of a dedicated chemistry manager. Such a framework has been shown to accurately capture the NOx emission evolution in a cost-effective manner with OpenNCC [4,6] for multiple LDI flametube configurations. The computational speedup of the MTS-FPV approach, as compared to finite-rate chemistry modeling for large kinetics mechanisms, enabled the timely completion of the parametric study reported in this paper.

3.1 Gas and Liquid Phase Properties for Average Jet-A (A2) Fuel

The baseline skeletal kinetics mechanism for modeling A2 fuel consisted of 41 species, with an additional 30 species to account for NOx related computations. Some details of the chemical and combustion properties of A2 fuel, as used in the HyChem kinetics mechanism [8], are shown in Table 2. The CANTERA [11] computed values for flame temperature, ignition delay and flame for supersonic cruise conditions ($P_3= 15.9\text{bar}$, $T_3=884\text{K}$, $T_4=1824\text{K}$), are also shown in Table 2. All gas-phase thermodynamic and transport properties used for both the CANTERA and OpenNCC modeling were those that accompanied the HyChem skeletal kinetics mechanism. In this study, some temperature-dependent liquid properties (density, heat capacity, viscosity, vapor pressure, latent heat) for A2 fuel were implemented from the work of Esclapez [12].

Gas Fuel Property / Kinetics [8]	A2
Chemical Formula (Average)	$C_{11.4}H_{21.7}$
H/C ratio	1.90
Derived Cetane Number (DCN)	47
Net heat of Combustion (MJ/kg)	42.8
Chemical Formula (Modeled)	$C_{11}H_{22}$
Non-NOx Species (Skeletal Kinetics)	41
Species for NOx Kinetics	30
Adiabatic Flame Temperature, K	1824
Ignition Delay Time, ms	24.9
Flame Speed, cm/s	32.6

Liquid Fuel Property	A2
Molecular Weight (g/g-mole)	154.1
Normal Boiling Point (K)	489.5
Density at 1bar (kg/m^3)	791.5
Critical Temperature (K)	760.4
Critical Pressure (bar)	18.2
Heat of Vaporization (kJ/kg)	310.0
Critical Volume ($\text{cm}^3/\text{g-mole}$)	700.4

Table 2. Gas phase and liquid properties of 'average Jet-A' (A2) fuel used in OpenNCC

3.2 Spray Modeling for Average Jet-A (A2) Fuel

The MTS-FPV chemistry model using a pre-computed flamelet table based on HyChem skeletal-kinetics for A2 fuel, was coupled with OpenNCC’s lagrangian-spray approach to perform multiphase computations for the radial-airflow injection flametube shown in figure 2. Spray modeling for the main injection elements assumed that the annular fuel sheet exiting the injector breaks up into 8 discrete streams of uniform liquid mass and momentum. Each stream was modeled as a 5 solid cone containing 8 droplet groups with an SMD of $8\mu\text{m}$. The initial droplet injection velocity and temperature were 5m/s and 300K, respectively. The pressure-atomizing simplex injection element (pilot) located at the center of was modeled as a 60° hollow cone of 10° thickness. Spray particles were injected as 16 streams

at an injection velocity of 28m/s, and an SMD of 8 μ m with a mass distribution across 8 droplet group sizes. The droplet size distribution for injected particles was prescribed by the following correlation equation[7]:

$$\frac{\delta n}{n} = 4.21 \times 10^6 \left[\frac{d}{d_{32}} \right]^{3.5} e^{-16.98 \left[\frac{d}{d_{32}} \right]^{0.4}} \frac{\delta d}{d_{32}} \quad (1)$$

Here n is the total number of droplets, d_{32} is the Sauter mean diameter (SMD), δn is the number of droplets in the size range between d and $d + \delta d$.

3.3 OpenNCC Simulation for Liner-Cooling Flow Parametric Study

Several tetrahedral meshes of increasing mesh densities were generated for the LDI radial-airflow combustor with LLNL's CUBIT mesh generation software [13]. Non-reacting solutions were computed with OpenNCC for each mesh and the predicted 'effective area' (ACd) for the Pilot injector and the Main injectors were compared with experimental data. The mesh-convergence criterion was set to a '10% or less difference between predicted and measured ACd values' for the flametube. The converged mesh consisted of 13.7M tetrahedral elements and 2.5M nodes.

The OpenNCC CFD computations for all four liner cooling flow rates were performed for a supersonic cruise condition of $P_3=15.9\text{bar}$ (234psi), $T_3=884\text{K}$ (1132F), $\phi=0.43$ (FAR=0.0295), $T_4=1824\text{K}$ and $\Delta p=3.5\%$. The airflow inlet boundaries for the Pilot and Main injectors, and the cooling hole inlets, were modeled with fixed total pressure and total temperature conditions derived from the P_3 and T_3 for the cruise condition. The outflow boundary was modeled with a fixed static-pressure for subsonic outflow based on the specified Δp between the inflow and outflow of the combustor. No-slip, adiabatic flow conditions were imposed at all solid surfaces.

The liner-cooling flow rates for each of the four CFD cases were set as fixed mass-flow, wall-injection boundary conditions at the top and bottom liner walls of the flame tube (see figure 3). The total liner-cooling flow specified for each case was split between the top and bottom walls at a 5:3 ratio, which corresponded to the surface area ratio of the outer and inner liner walls, respectively. The liner cooling flow was distributed uniformly across the surface of each liner wall in a direction normal to the wall, at the same temperature as the primary airflow ($T_3=884\text{K}$). Periodic boundary conditions were imposed on the angled left and right surfaces of the combustor in order to model a 1/16th sector of an annular combustor.

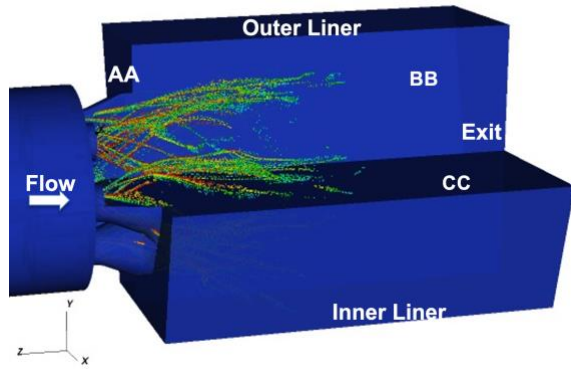


Figure 3. Schematic of flame-tube configuration showing nominal fuel spray distribution, liner surfaces for cooling flow injection, and cross-sections (AA, BB and CC) for CFD results.

The initial conditions for the CFD computations represented static air at P_3 and T_3 in the entire computational domain. RANS CFD with a 2nd-order accurate central-differencing operator and 4-stage explicit Runge-Kutta time-integration was used to establish a converged non-reacting flow-field for the 'baseline' condition of 0% cooling flow-rate. The non-reacting RANS solution was then used to generate a time-accurate solution using a dual-time stepping approach, coupled with the Time-Filtered Navier Stokes (TFNS) solver of OpenNCC. The physical time-step was set to 1e-6s, and 10000 time-steps were computed to obtain the non-reacting TFNS solution. A reacting-flow, TFNS

solution using the MTS-FPV modeling approach was then obtained, with initiation of fuel-injection and two-phase computations, and artificial ignition of the fuel-air mixture downstream of each of the injectors. Reacting flow solutions with four additional progress variables for NOx computations were then initiated, and a time-averaged converged solution for NOx mass-fractions and EINOx was obtained for the 'baseline' design.

The parametric study for the 7%, 15% and 56% liner-cooling rates were each initialized with the converged reacting flow solution from the 'baseline' 0% liner-cooling flow solution. This approach ensured that the comparison of EINOx values for each of the liner-cooling flow rates was done at the identical final solution time of 20m-s. The 7% and 15% cases represent optimistic lower limits of liner cooling flows for practical modern aircraft gas turbine combustors. The 56% liner cooling flow case, which raises the dome FAR to an "off-design" values, was studied to establish a nominal higher bound for EINOx for the current design operating at CST cruise conditions.

In order to maintain a constant global fuel/air ratio (FAR) for each case, the specified fuel flow rate for the pilot injector and six main injectors was increased in proportion to the increase in liner cooling flow rate. As the airflow rate through the combustor dome face was held constant, the increase of n% in fuel flow rate for say n% liner flow rate, thus raised the local fuel-air ratio (FAR) at the dome face by n%. The increase in local FAR translates to an increase in local flame-temperature near the dome face (see table 3), which would be expected to increase NOx production due to the increased residence time of hotter combustion products in the flame tube.

Liner Cooling Flow Rate (% of dome airflow rate)	Dome Temperature (K) (increase %)	Dome FAR (fuel/air ratio)
0% (Baseline)	1824 (Baseline)	0.0295
7.5%	1880 (3%)	0.0317
15%	1939 (6%)	0.0339
56%	2275 (25%)	0.0460

Table 3. Comparisons of EINOx for supersonic cruise at $P_3= 15.9\text{bar}$ (234psi), $T_3=884\text{K}$ (1132F), FAR=0.0295.

3.4 OpenNCC CFD Predictions: Axial Velocity, Temperature and NOx Profiles

One primary goal of the CFD parametric study was to evaluate the differences in NOx emissions for a radial airflow injector design at supersonic flight conditions with different liner-cooling flow rates. Based on OpenNCC computations, a co-rotating radial-airflow design was selected for the liner-cooling flow rate study in this paper as it had been predicted to have 20% lower EINOx as compared to a radial inflow counter-rotating configuration [6]. The impact of three different cooling flow rates (7.5%, 15% and 56%) on aerodynamics, flame structure and NOx production in the co-rotating radial airflow configuration are summarized in this section.

The OpenNCC two-phase reacting flow results were post-processed with VisIt [11] to produce contour plots of axial velocity, temperature and NO mass-fraction at several cross-sections of a newly designed radial-airflow injection LDI flametube. The CFD contours represent time-averaged values of the final flow-through cycle for each of the four liner cooling flow rates studied: 0%, 7.5%, 15% and 56% of the dome airflow rate of the flametube. The EINOx value for each of the four CFD cases is computed using the time-averaged value of the NO mass-fraction exit plane. In the current CFD configuration, the exit plane is located 150mm downstream of the combustor dome face.

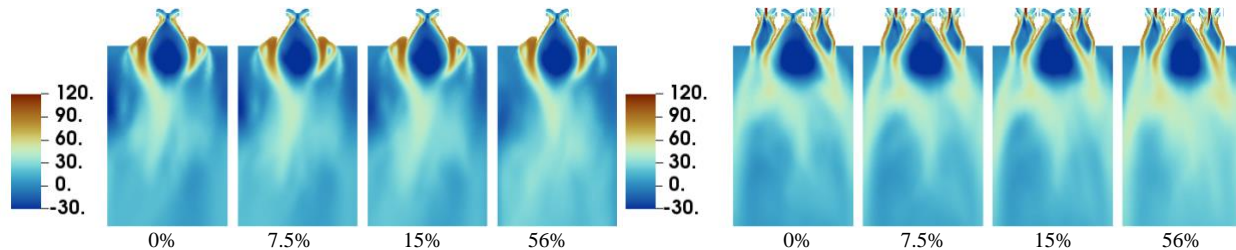


Figure 4. Axial velocity (m/s) contours for four cooling flow-rates. 'Pilot-only' section with liner walls (left), and 'pilot with mains' section (right)

The axial velocity contours (figure 4) in the 'pilot-only' plane show the presence of a very stable recirculation zone behind the Pilot injector, which is relatively unaffected by the increase in liner cooling flow. However, the mixing of the flow downstream does seem to be influenced by the increase in cooling flow rate, particularly for the 56% case. The 'pilot with mains' cross-section shows strong recirculation zones in the diverging section of each main injection element. The pilot recirculation zone in this cross-section is much less compact than in the 'pilot-only' cross-section because of the much weaker axial momentum of the adjacent flowfield. There are almost no effect of the cooling flow rates on the aerodynamics in the 'pilot with mains' section, primarily because this section lies midway between the upper and lower liner walls.

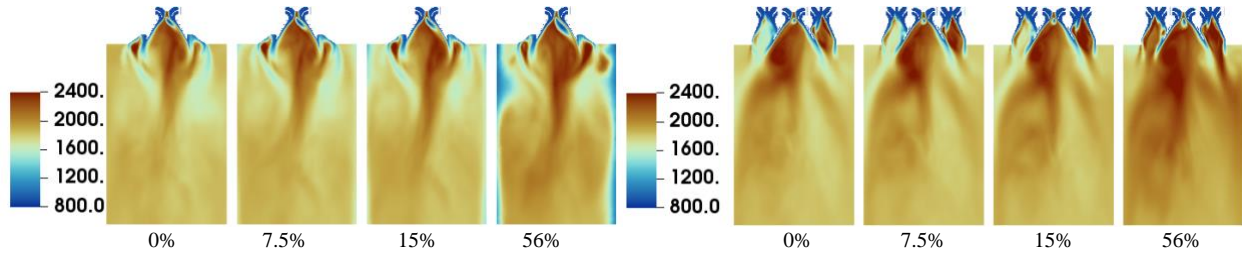


Figure 5. Temperature (K) contours for four cooling flow-rates. 'Pilot-only' section with liner walls (left), and 'pilot with mains' section (right)

The temperature contours (figure 5) in the 'pilot-only' plane show the significant effect of the increasing the local fuel-air ration and flame temperature near the dome as the cooling flow rate increases. The temperature increase in the primary flame region for the 7.5% and 15% cooling flow rates seems marginal, partly because the equilibrium flame temperature increase is only 3% and 6%, respectively. The 'pilot with mains' cross-section also shows relatively small temperature increases behind the pilot and both main elements for the 7.5% and 15% cases. The effect of the aerodynamics (figure 4) is clearly seen on the spreading of the flame behind the pilot element: a very compact flame in the 'pilot-only' cross-section and a relatively diffuse flame in the 'pilot with mains' section. highest which is relatively unaffected by the increase in liner cooling flow. As expected, the 56% cooling-flow rate case shows significant increases in flame temperatures in both cross sections.

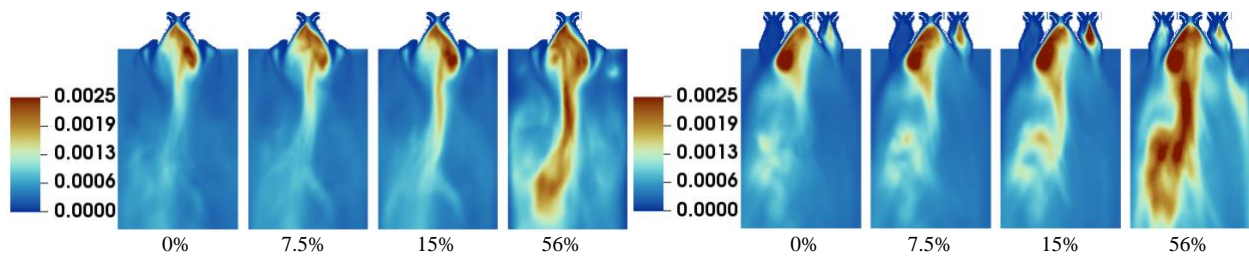


Figure 6. NO mass-fraction contours for four cooling flow-rates. 'Pilot-only' section with liner walls (left), and 'pilot with mains' section (right)

The NO mass-fraction contours (figure 6) for both the 'pilot-only' and 'pilot with mains' sections show that a majority of the NO_x is produced behind the pilot element as compared to the main injector elements. As expected, the significantly higher temperature regions behind the pilot injector (figure 5) are directly responsible for the NO_x production. The EINO_x values for the 3% and 6% increase in dome temperature, corresponding to the 7.5% and 15% liner cooling cases, were computed to be 8% and 21% higher than the baseline case, respectively. This represents a non-linear increase of EINO_x with increase in dome temperature in the flametube. As expected, the 56% liner cooling flow case with an 'off-design' fuel-air ratio has 58% higher EINO_x as compared to the baseline case. The 56% cooling flow case represents a nominal upper-bound of EINO_x for this flametube configuration. Based on the predicted EINO_x results from the CFD parametric study, a correlation equation was derived for the dependence of the increase in EINO_x (ΔNO_x , %) relative to the baseline, with the liner cooling flow rate (CFR, %):

$$\Delta\text{NO}_x = -0.016*(\text{CFR})^2 + 2.016*\text{CFR} - 5.944 \quad \{1\}$$

The ΔNO_x correlation may be useful to predict the variation in EINO_x with liner cooling-flow rate for future LDI combustor designs at similar supersonic cruise operating conditions.

Even though the pilot and main injection elements operate at identical fuel air ratios, the mixture behind the pilot element burns very differently as compared to the main elements. The pilot element, fueled by a pressure atomizing fuel injector, evaporates the fuel much more quickly than pre-filming injectors which fuel the main injection elements. The fuel-air mixing and heat release behind the pilot element is thus relatively rapid in the vicinity of the fuel injection location. However, considerable non-uniformity in the circumferential temperature distribution is predicted within the diverging section of the pilot venturi where the primary burning is occurring. The combination of rapid heat release and non-uniform temperature distribution, combined with increased residence time for high temperature combustion products is one likely explanation for much higher NO_x production in the central pilot injection element of the seven-element combustion module.

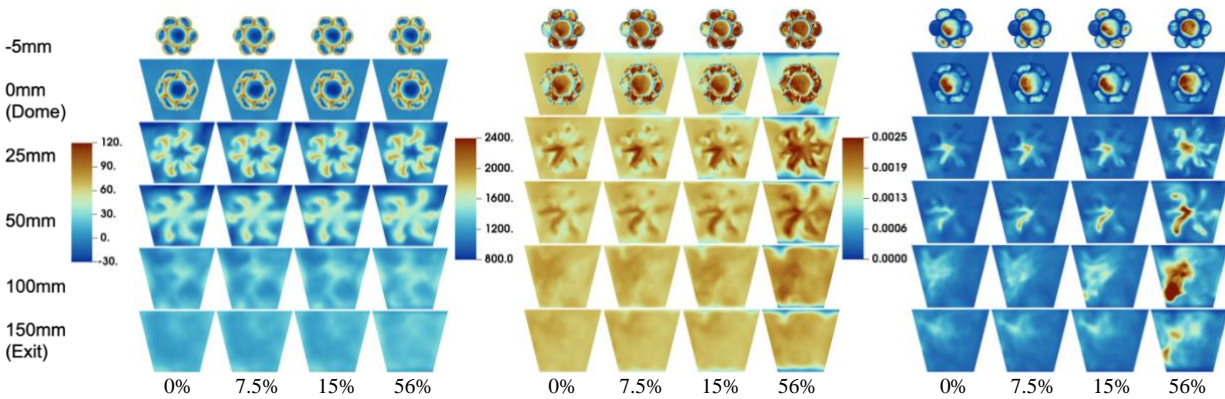


Figure 7. Liner cooling flow-rate effects on axial velocity (m/s, left), temperature (K, center) and NO mass-fraction (right) at six axial cross sections along the length of the flame-tube.

Figure 7 represents a summary of the development of the combustor flowfield as it progresses axially from the dome face to the exit plane of the flametube. Contours of axial velocity, temperature and NO mass-fraction are shown at six axial cross sections chosen to best represent the significant features of each of the four liner-cooling flow rate variations. The strong recirculation zones created by the air swirlers of the six main elements and the pilot element are shown to disappear near the 25mm location downstream of the dome. The 'six-prong pattern' formed by the six mains finally mixes out with the pilot flow near the 100mm location. The recirculation zones and shear layers formed behind all the injection elements strongly influence the flame structure, flame length and NO_x production for each of the four liner flow-rates computed with OpenNCC CFD. The flow and flame characteristics for the 0%, 7.5% and 15% liner flow-rate cases are qualitatively similar to each other. As expected, the 56% liner flow-rate case develops significant gradients in temperature and NO mass-fraction downstream of the 25mm location as the relatively cold flow from the upper and liner walls starts mixing with the core combustion products.

4.0 Summary and Significance of CFD Parametric Studies

A summary comparison of CFD predictions of EINO_x (g of NO_x per kg of fuel) for the 0% (baseline), and the 7.5%, 15% and 56% liner-cooling flow rate conditions is shown in Table 4. The EINO_x emissions trends can be summarized as below:

1. As expected, the CFD predictions of NO_x emissions increase as the dome FAR increases with an increase in liner-cooling flow rates.
2. CFD predictions of NO_x emissions are expected to approximately increase by approximately 10% for each 7.5% increase in liner cooling flow rate for the radial-swirler airflow configuration studied in this paper.
3. The predicted trend of increase in EINO_x with increase in liner cooling flow rates for the current LDI-4 configuration matches the EINO_x trend shown in experimental data for an LDI-3 configuration [5].

Liner Cooling Flow Rate (% of dome airflow rate)	Increase in EINOx (g-NOx/kg-fuel)	Dome Temperature (K) (increase %)	Dome FAR (fuel/air ratio)
0% (Baseline)	-	1824 (Baseline)	0.0295
7.5%	8.3%	1880 (3%)	0.0317
15%	20.8%	1939 (6%)	0.0339
56%	58.3%	2275 (25%)	0.0460

Table 4. Comparisons of EINOx for supersonic cruise at $P_3= 15.9\text{bar}$ (234psi), $T_3=884\text{K}$ (1132F), FAR=0.0295.

Combustor liner design for aircraft engine applications remains an important area of research for the gas-turbine community. Significant investments continue to be made by NASA and OEMs in the development of ceramics and thermal barrier coatings (TBCs) for combustor components. With advances in ceramics and TBCs, engine designers can reduce the amount of total engine airflow that is assigned for liner cooling from the current 20-30% range. The parametric study reported in this work was successful in providing insights into the impacts of liner-cooling air-flow rates on the aerodynamics, flame structure and NOx emissions of an improved Lean Direct Injection (LDI) design. While the current parametric study focused on a cruise condition for a commercial supersonics aircraft application, the OpenNCC CFD methodology could also be used to explore LDI combustor design for subsonic aircraft applications. In future work, OpenNCC will be used to predict emissions trends for two recently re-designed and experimentally tested LDI injector modules at NASA Glenn Research Center.

5.0 Acknowledgements

This research was funded by the Commercial Supersonic Technology (CST) Project under NASA’s Advanced Air Vehicles Project (AAVP). Computational resources were provided by the NAS Supercomputing at NASA Ames Research Center.

6.0 References

- [1] Ajmani, K., Lee, P., Chang, C.T. and Kudlac, M.T., “CFD Evaluation of Lean-Direct Injection Combustors for Commercial Supersonics Technology,” AIAA Paper 2019-4199, AIAA Propulsion and Energy Conference 2019, July 2019, Indianapolis IN.
- [2]. Ajmani, K., Lee, P., Mongia, H.C. and Tacina, K.M., “[CFD Predictions of N+3 Cycle Emissions for a Three-Cup Gas Turbine Combustor](#),” AIAA Paper 2018-4957, 54th AIAA Joint Propulsion Conference, July 2018, Cincinnati OH.
- [3] Ajmani, K., and Chang, C.T., “CFD Evaluation of Aviation Fuels for Commercial Supersonics Technology,” AIAA Paper 2022-1105, AIAA Scitech Meeting 2022, January 2022, San Diego CA.
- [4] Ajmani, K., and Moder, J.M., “CFD Evaluation of Sustainable Aviation Fuels for Commercial Supersonics Technology,” 13th US National Combustion Meeting, Paper 180AFE-0190 March 2023, College Station TX.
- [5] Tacina, K.M., Podboy, D.P., Lee, P., and Dam, B., “Gaseous Emissions Results from a Three-Cup Flametube Test of a Third-Generation Lean Direct Injection Combustor Concept”, ISABE 2017, Edinburgh UK.
- [6] Ajmani, K., and Moder, J.M., “CFD Evaluation of Radial Airflow Lean Direct Injectors for Commercial Supersonics Technology,” 2024 Spring Technical Meeting of the CSSCI, Paper 235AFEQ-0036, May 2024, Cleveland OH.
- [7] M.S. Raju, “LSPRAY-IV: A Lagrangian Spray Module,” NASA CR-2012-217294.
- [8] H. Wang, R. Xu, K. Wang, C.T. Bowman, D.F. Davidson, R.K. Hanson, K. Brezinsky, F.N. Egolfopoulos, A physics-based approach to modeling real-fuel combustion chemistry - I. Evidence from experiments, and thermodynamic, chemical kinetic and statistical considerations, *Combustion and Flame* 193 (2018) 502-519.

[9] Muralidharan, B., Zambon, A., Hosangadi, A., and Calhoon, W.H. Jr, "Application of a progress variable based approach for modeling non-premixed/partially premixed combustion under high-pressure conditions," AIAA Paper 2018-4560, AIAA Joint Propulsion Conference 2018, July 2018, Cincinnati OH. DOI: 10.2514/6.2018-4560

[10] Zambon, A. C., B Muralidharan, B., Hosangadi, A., and Ajmani, K., "[A Multi-Time-Scale Flamelet Progress Variable Approach in OpenNCC for Predicting NOx Applied to Commercial Supersonic Transport Combustor Designs](#)," AIAA Propulsion and Energy Forum 2020-3896, August 2020.

[11] David G. Goodwin, Harry K. Moffat, Ingmar Schoegl, Raymond L. Speth, and Bryan W. Weber. *Cantera: An object-oriented software toolkit for chemical kinetics, thermodynamics, and transport processes*. <https://www.cantera.org>, 2022. Version 2.6.0. doi:10.5281/zenodo.6387882

[12] Lucas Esclapez, Peter C. Ma, Eric Mayhew, Rui Xu, Scott Stouffer, Tonghun Lee, Hai Wang, Matthias Ihme, "Fuel effects on lean blow-out in a realistic gas turbine combustor," *Combustion and Flame*, 181 (2017). <https://dx.doi.org/10.1016/j.combustflame.2017.02.035>

[13] Teddy D. Blacker, Steven J. Owen, Matthew L. Staten, William R. Quadros, Byron Hanks, Brett W. Clark, Ray J. Meyers, Corey Ernst, Karl Merkley, Randy Morris, Corey McBride, Clinton Stimpson, Michael Plooster, and Sam Showman. *CUBIT Geometry and Mesh Generation Toolkit 15.2 User Documentation*. United States: N. p., 2016. Web. <https://doi.org/10.2172/1457612>

[14] Hank Childs, Eric Brugger, Brad Whitlock, Jeremy Meredith, Sean Ahern, David Pugmire, Kathleen Biagas, Mark Miller, Cyrus Harrison, Gunther H. Weber, Hari Krishnan, Thomas Fogal, Allen Sanderson, Christoph Garth, E. Wes Bethel, David Camp, Oliver Rubel, Marc Durant, Jean M. Favre, and Paul Navr, "VisIt: An End-User Tool for Visualizing and Analyzing Very Large Data," *High Performance Visualization--Enabling Extreme-Scale Scientific Insight (2012)*, 357-372.